Electronic Supplementary Information (ESI)

Unleashing the Potential of Li-O_2 Batteries with Electronic Modulation and Lattice Strain in Pre-Lithiated Electrocatalysts

Zhengcai Zhang,[a†] Dulin Huang,[a†] Shuochao Xing,[a] Minghui Li,[a] Jing Wu,[a] Zhang Zhang,[a] Yaying Dou,[a,b*] Zhen Zhou[a*]

1. Interdisciplinary Research Center for Sustainable Energy Science and Engineering (IRC4SE^2), School of Chemical Engineering, Zhengzhou University, Zhengzhou 450001, China
2. Key Laboratory of Advanced Energy Materials Chemistry (Ministry of Education), College of Chemistry, Nankai University, Tianjin 300071, China

*Corresponding Author(s): Yaying Dou: yydou@zzu.edu.cn.
Zhen Zhou: zhenzhou@zzu.edu.cn

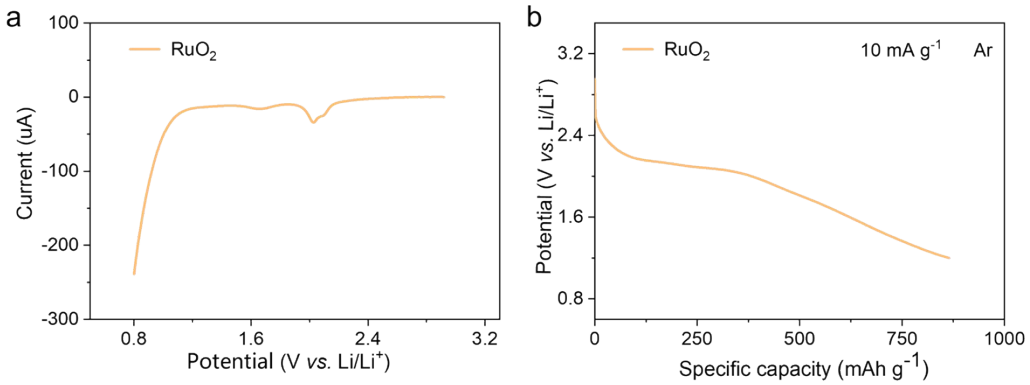

Fig. S1 (a) LSV curves of RuO_2 with a scan rate of 0.05 mV s^{-1} and (b) discharge profile of RuO_2 at a current density of 10 mA g^{-1}.

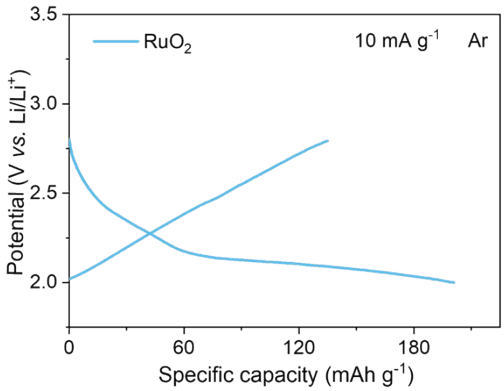

Fig. S2 The initial discharge-charge potential profiles of RuO_2 as the work electrode with Li metal as the counter electrode at a current density of 10 mA g^{-1}.

The theoretical specific capacity of RuO_2 is approximately 201 mAh g^{-1}, corresponding to the insertion of 1 mol of Li^+ into 1 mol of RuO_2. As shown in Figure S2, the coulombic efficiency of the 1st cycle is ~ 65%, indicating 35% irreversible capacities occurred during the lithiation, which mainly corresponds to Li^+ without inserting RuO_2. In this case, we assume that the coulombic efficiency is the same when the RuO_2 electrode is cycled between different voltage windows. Discharge experiments were conducted at a current density of 10 mA g^{-1} for 4, 8, 12, and 16 hours, resulting in specific capacities of 40, 80, 120, and 160 mAh g^{-1}, respectively. Considering the 35% irreversible capacities occurred during the lithiation, the Li^+ concentration (x) in Li_xRuO_2 was determined to be 0.13, 0.27, 0.39, and 0.52, respectively. Importantly, even after 16h discharge, the terminal voltage remained above 2 V, indicating continuous lithium intercalation throughout the entire process.

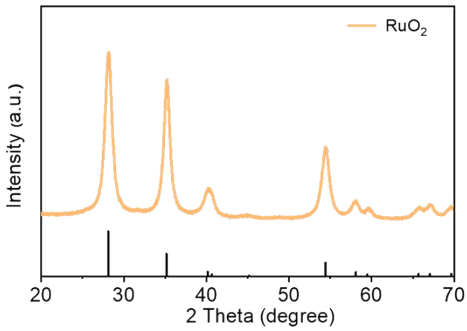

Fig. S3 XRD patterns of pristine RuO_2.

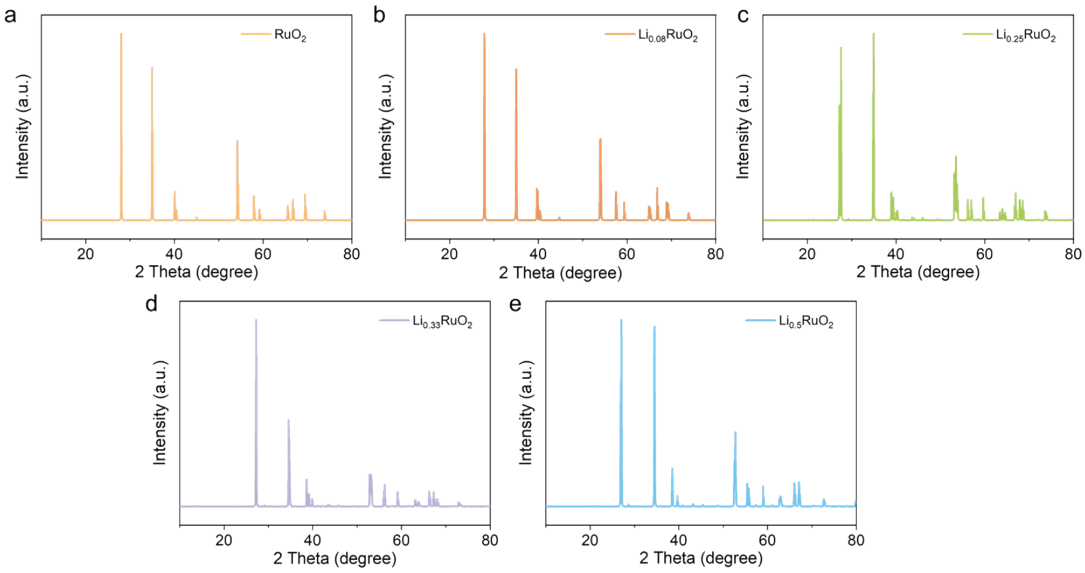

Fig. S4 Simulated XRD diffraction patterns of Li_xRuO_2 with different Li^+ concentrations based on theoretical calculations.

Tab. S1 Lattice parameters of the Li_xRuO_2 obtained by DFT calculations.

Samples	Lattice constant (Å)	Volume (Å^3)
RuO_2	a=b=4.501, c=3.120	63.21
$Li_{0.08}RuO_2$	a=4.52, b=4.542, c=3.111	63.87
$Li_{0.25}RuO_2$	a=4.584, b=4.624, c=3.097	65.65
$Li_{0.33}RuO_2$	a=4.601, b=4.662, c=3.121	66.95
$Li_{0.5}RuO_2$	a=4.669, b=4.676, c=3.128	68.29

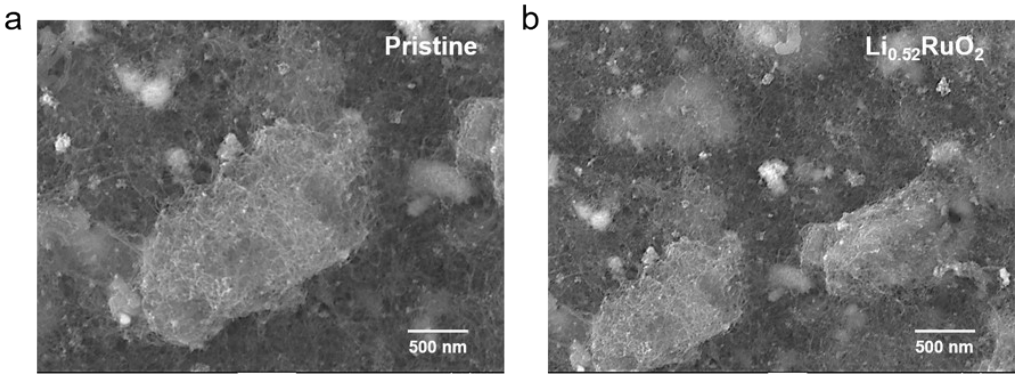

Fig. S5 SEM images of (a) pristine RuO_2 and (b) $Li_{0.52}RuO_2$ electrodes.

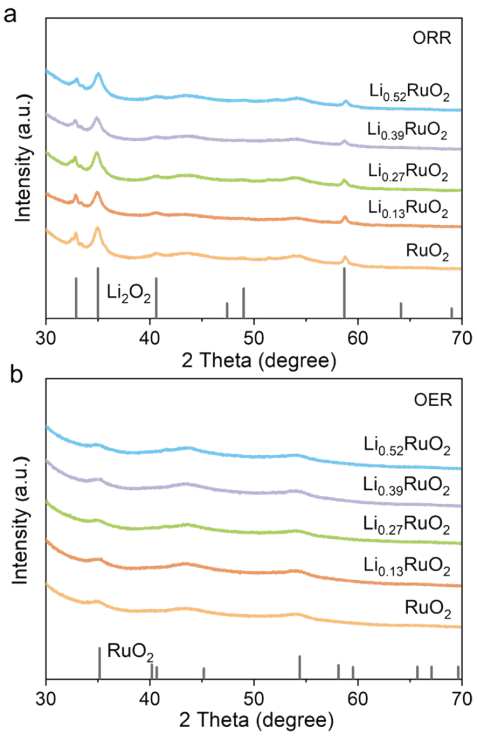

Fig. S6 XRD patterns of Li-O_2 batteries with RuO_2 and Li_xRuO_2 cathodes after discharge (a) and recharge (b).

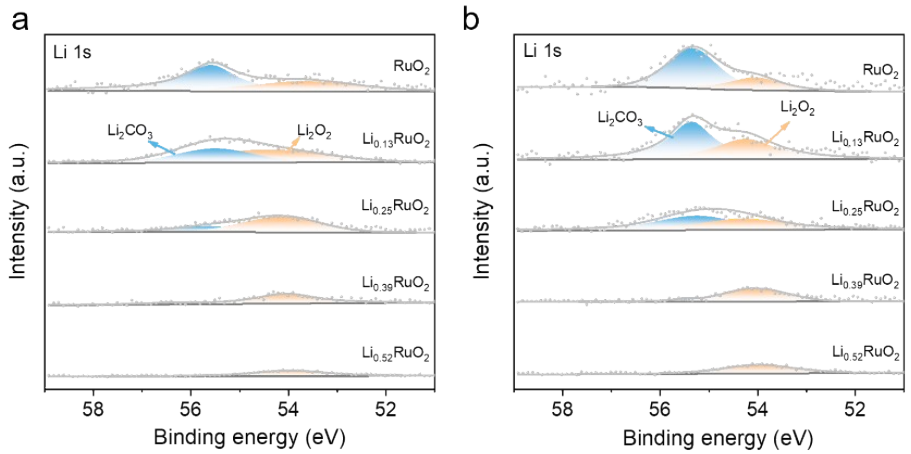

Fig. S7 Li 1s XPS of oxygen cathodes after the 1st (a) and 10th (b) recharge.

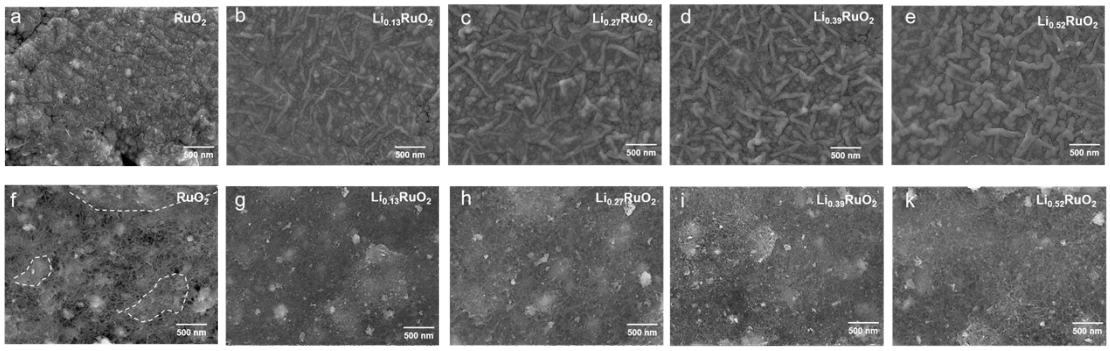

Fig. S8 SEM images of Li-O_2 batteries with RuO_2 and Li_xRuO_2 cathodes after discharge (a-e) and recharge (f-k).

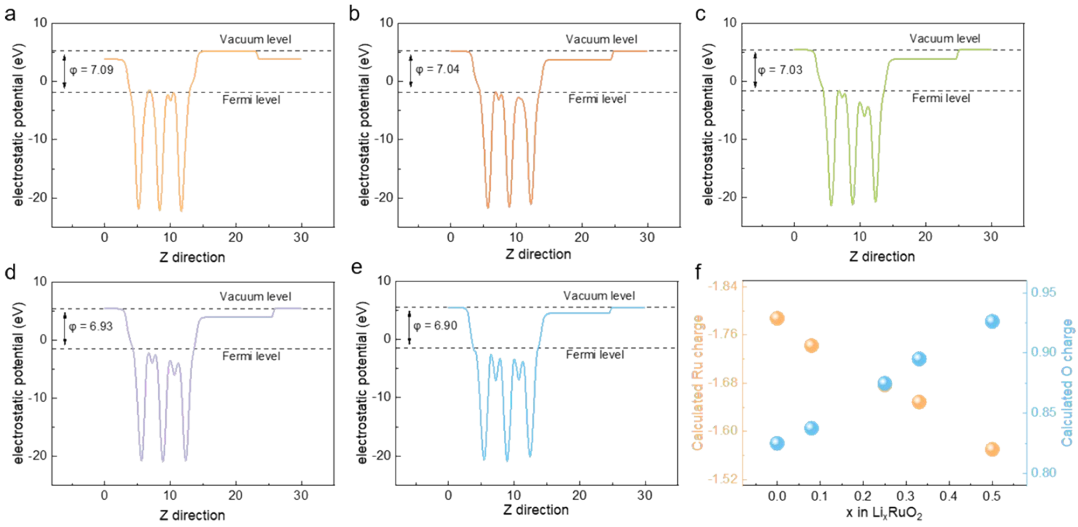

Fig. S9 (a-e) The electrostatic potential and work function on the catalyst surface of Li_xRuO_2 (x=0, 0.08, 0.25, 0.33, 0.5) embedded at different Li concentrations. (f) The electron transfer of Ru and O in the catalyst Li_xRuO_2 with different Li^+ concentrations.

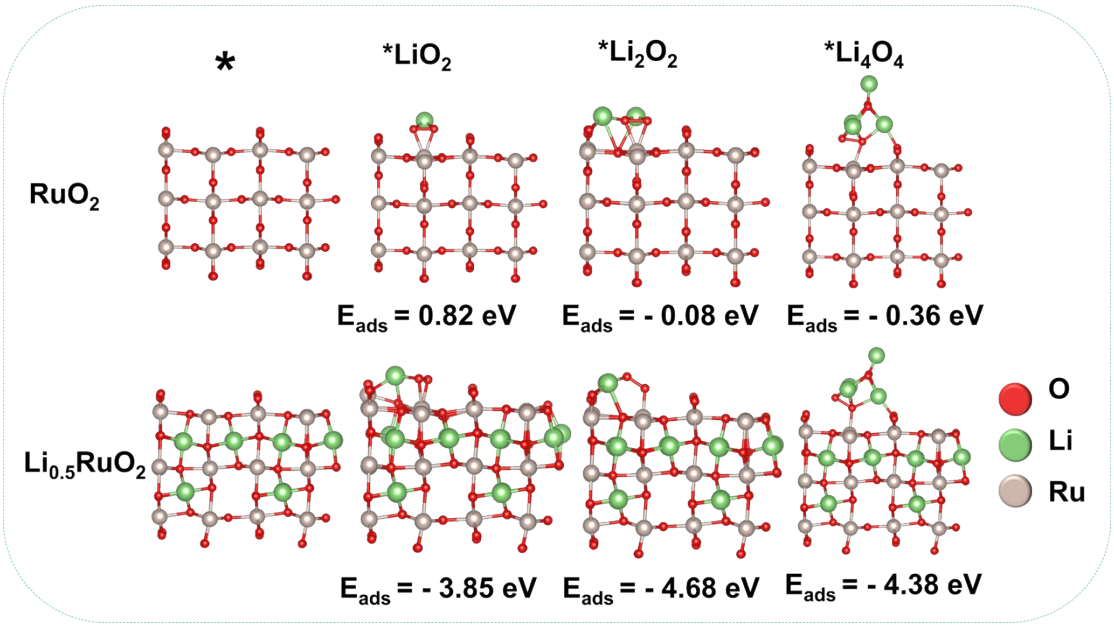

Fig. S10 The structure models and corresponding adsorption energies of various Li-O species on RuO_2 and $Li_{0.5}RuO_2$ (110) planes.

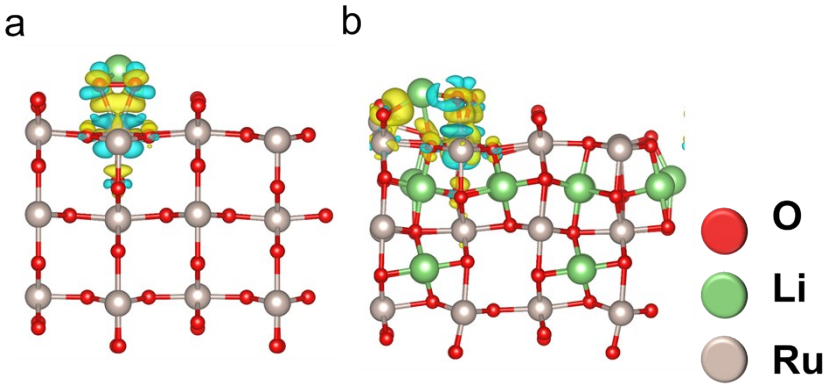

Fig. S11 Charge density difference plots of LiO_2 on (a) RuO_2 (110) or (b) $Li_{0.5}RuO_2$ (110), with yellow denoting the increased charge and cyan the decreased charge.

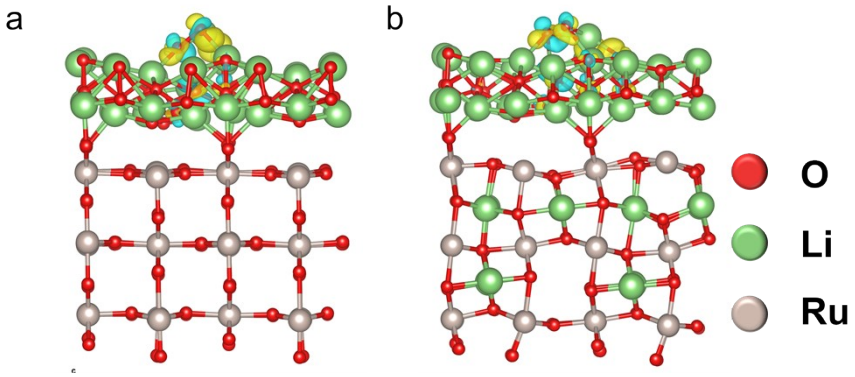

Fig. S12 Charge density difference plots of LiO_2 on (a) RuO_2 (110) or (b) $Li_{0.5}RuO_2$ (110) covered by Li_2O_2, with yellow denoting the increased charge and cyan the decreased charge.